PHILIPPINE ENGINEERING JOURNAL
PEJ 2014; Vol. 35, No. 1: 13-24

AN EXPERIMENTAL INVESTIGATION ON THE PERFORMANCE OF A VERTICAL AXIS WIND TURBINE IN STEADY WIND

Jonathan Mark Edwards[1], Louis Angelo Danao[2] and Okeoghene Eboibi[3]
[1] Department of Civil and Structural Engineering
University of Sheffield, Sheffield, United Kingdom
[2] Department of Mechanical Engineering
University of the Philippines, Diliman, Quezon City, Philippines
[3] Department of Agricultural Engineering
Delta State Polytechnic, Ozoro, Nigeria

ABSTRACT

An experimental study was carried out into the performance of a wind tunnel scale vertical axis wind turbine (VAWT) under steady wind conditions. Wind speed tested was 7m/s, giving a Reynolds number of around 75,000. The power coefficient (CP) of the VAWT over a wide range of λ reveals a negative trough from $\lambda = 1$ up to $\lambda = 3$ with the lowest CP of –0.11 at $\lambda = 2.4$. Beyond $\lambda = 3$ the CP rises to a maximum of 0.21 at $\lambda^* = 4.0$ after which it falls close to zero at $\lambda = 5$. This CP profile is typical of the scale of the VAWT tested where a negative trough is present mostly due to high zero–lift drag that hampers the ability of the rotor to generate positive torque at low λ and self–start. The negative trough is observed to slowly diminish as wind speeds, and consequently, Reynolds number increases.

1. INTRODUCTION

A general consensus has been made in the recent years that the effects of climate change are becoming more severe and prevalent [1]. The main cause of the increasing rate of undesirable climatic conditions has been identified as greenhouse gas emissions from the burning of fossil fuels used primarily for energy generation and transportation purposes. For this reason, there has been a pressing need to reduce emissions through the use of technologies that are capable of extracting energy from the environment whilst being non–polluting and sustainable. Several alternative sources to fossil fuels have been identified: tidal, solar, biomass, and wind. These are branded as 'renewables' and have attracted significant research attention in the past decades. Of these renewable sources, the contribution of wind to the total energy generation of the U.K. has been steadily rising over the last few years and has seen the leading renewable technology for electricity generation with 45% for onshore [2]. Wind has also been the leading renewable technology for electricity generation with 45% of the total 2011 renewable production. Despite these numbers, the total consumption of electricity from renewable sources only account for 9.4%. And the proportion of wind in the overall consumption is very low at 0.7% [3]. As a result, further research is needed to increase the understanding of this renewable power source to promote its wider adoption.

Correspondence to: Louis Angelo Danao, Dept. of Mechanical Engineering, University of the Philippines, Diliman, Quezon City. Email: louisdanao@coe.upd.edu.ph.

Received: January 21, 2013
Accepted: May 21, 2014

Wind turbines can be classified into two general types: drag machines and lift machines. Drag machines generate forces through the creation of large separated flows. Blades tend to move slower than the wind. The most common application of these devices is in water pumping. In lift machines, the wind is made to follow a curved path as it passes about a rounded object. The turning of the fluid generates forces on the object, typically of an aerofoil profile, thus producing the required thrust. Blade speeds are most often greater than the wind speed and far exceeds what is possible in drag machines. Lift machines are thus more favorable from an energy production view point due to a greater potential for energy extraction.

There are two main methods of extracting energy utilizing the lift concept: horizontal axis wind turbines or HAWT and vertical axis wind turbines or VAWT. HAWTs have received significant research and development work over the decades giving them a well–established and mature technology base that makes them the preferred configuration in all large scale wind farm installations. VAWTs on the other hand have not been given the same attention. The complex aerodynamic and structural aspects of VAWT operation make their understanding and optimization difficult which is one of the reasons why they are less favored than their horizontal counterparts.

There are several points of contention on the use of VAWTs over HAWTs. The key point that prevails is the generally perceived superior performance of HAWTs over VAWTs. Nevertheless, VAWTs present a number of potential advantages over HAWTs when it comes to applications in the built/urban environment:

- easier maintenance because of the rotor's proximity to the ground. VAWTs are typically smaller in scale and mounted on masts that are many times shorter than conventional HAWT installations. Additionally, the rotor sits on a bearing and drives the generator below it.
- no need to yaw to the wind thus reducing the efficiency loss when tracking changes in wind direction.
- sound emissions are usually lower as they operate at lower tip speed ratios [4]. This can also reduce structural issues such as vibration that result from high centrifugal forces.
- potentially lower manufacturing costs due to the simplicity of the blade shape.
- better performance in skewed flow [5].

The work carried out in this study is intended to provide initial understanding on the performance of a wind tunnel scale VAWT. It is not the aim of this research to provide absolute values of VAWT performance that may be used for comparison to commercially available machines. The present work is limited to a VAWT that operates in much lower Reynolds numbers and has a scale that does not exist in the current market. The data presented is exclusively for a wind tunnel VAWT and as such the conclusions are only applicable to rotors of similar scale. Nevertheless, the methods and analyses presented may be transferable to larger scales.

2. METHODOLOGY

The University of Sheffield – Department of Mechanical Engineering's low–speed wind tunnel was used for the experiments. The tunnel is an open-circuit suction device with an axial fan located at the outlet (Figure 1). The wind tunnel has a total length of 8.5m, including the 3m long

test section. At the tunnel inlet, a honeycomb mesh (with cells 10mm wide and 100mm long) straightens the flow and breaks up any large scale flow structures present in the room. After the honeycomb downstream is a fine mesh screen with 1mm cell size that further breaks up flow structures smaller than the honeycomb cells and generates small scale turbulence that help even out the flow. A short settling section after the fine mesh permits turbulence and non-uniformities to dissipate, after which the flow is accelerated by a two way 6.25:1 contraction cone leading to the 1.2m high × 1.2m wide test section. A turbulence grid is placed at the inlet of the test section to generate turbulence at the VAWT test position of about 1% intensity. The tunnel fan was controlled via a variable frequency drive that allowed the precise setting of the fan speed in 1rpm resolution with a maximum speed of just over 900rpm theoretically producing wind speeds close to 25m/s. For the current work, structural safety reasons dictated a maximum of 10m/s to limit the aerodynamic forces generated in the VAWT.

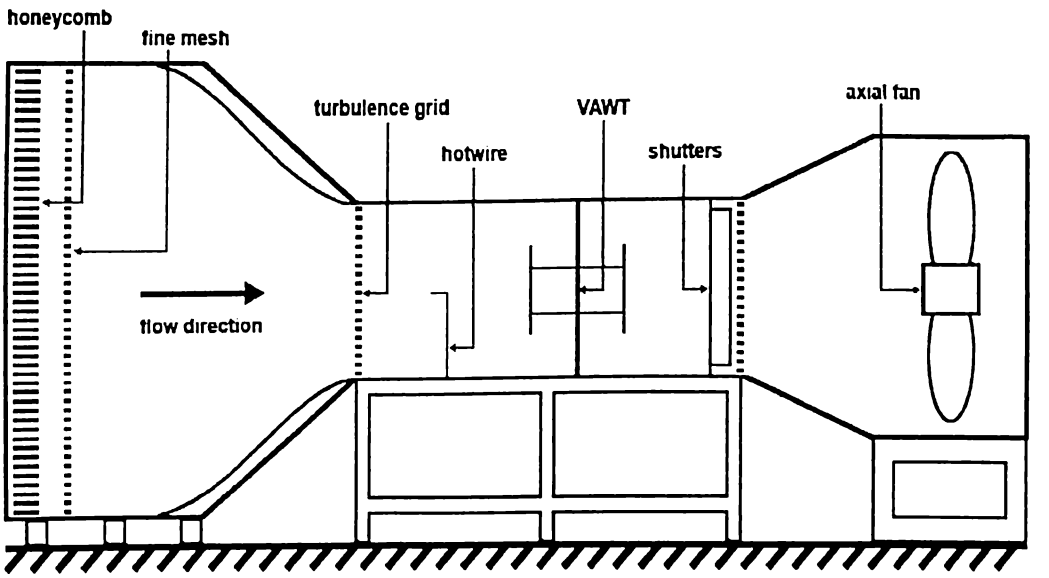

Figure 1. University of Sheffield wind tunnel facility.

The rotor is a straight–bladed VAWT with a 27mm diameter central shaft running through the top and bottom walls of the test section. The rotor is mounted in the centre of the test section area but is slightly downstream along the test section length. There are three NACA0022 blades with chord c = 0.04m each supported by two NACA0026 spokes of 0.03m chord at 25% and 75% blade length positions. A radial line from the VAWT centre to the blade perpendicularly intersects the chord at 0.5c. A hub is used to rigidly connect the support arms to the central shaft. The rotor diameter R is 0.35m and the blade span L is 0.6m giving the VAWT a solidity of $\sigma = 0.34$ following the conventional definition ($\sigma = Nc/R$) and a wind tunnel blockage ratio of 0.29 (2RL/A, where A: test section area). Figure 2 details the final design of the rotor.

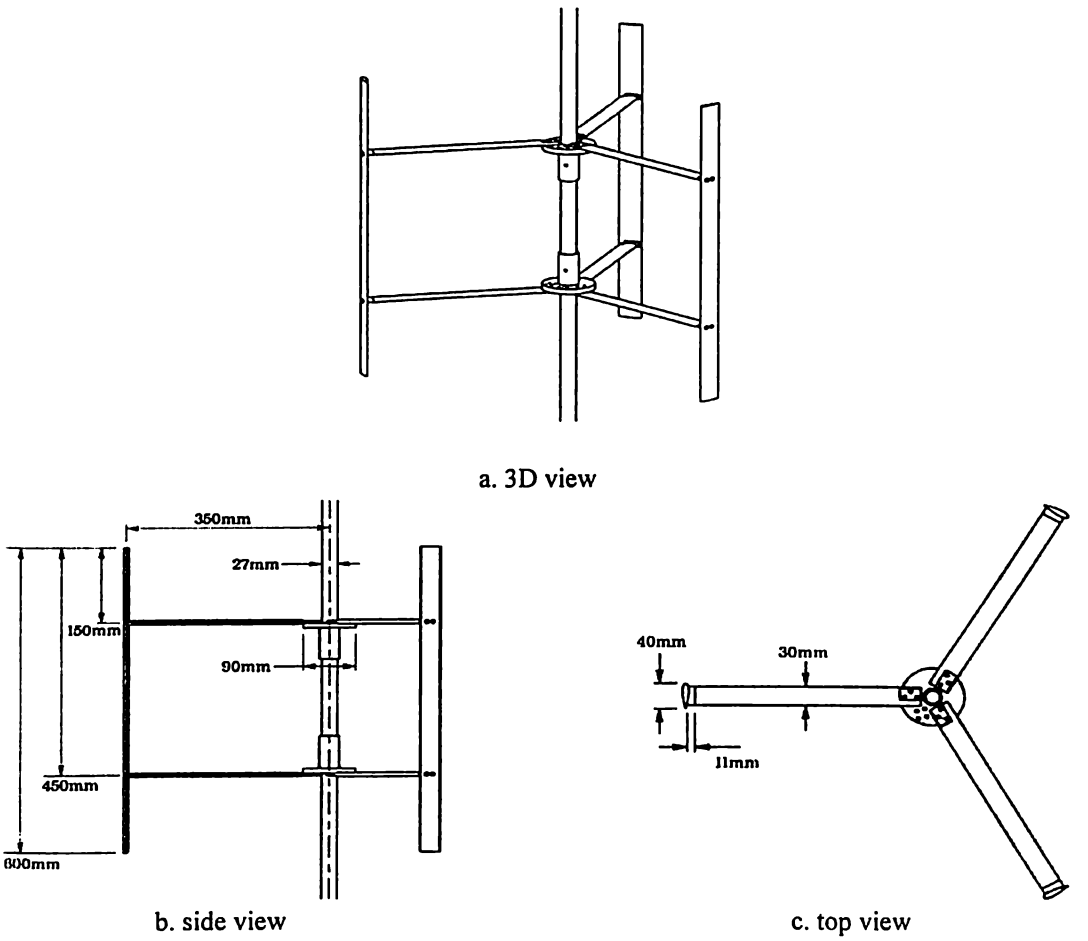

a. 3D view

b. side view

c. top view

Figure 2. VAWT rotor design.

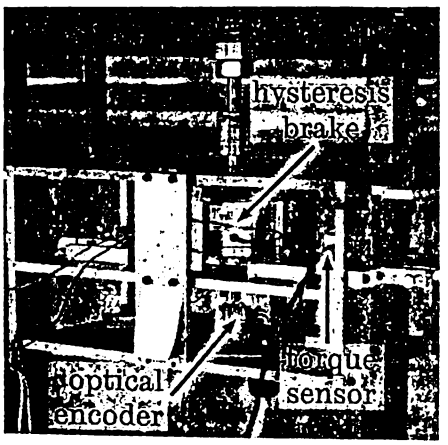

Figure 3. Torque and rpm measurement assembly.

To measure the rotor rotational velocity, an Avago optical encoder (model: AEDA-3300-TAM) with 3000 pulses per revolution was used. The encoder output was connected to a National Instruments BNC 2090 connector block. A National Instruments PCI–6220 data acquisitions card interfaced the connector block to a standard personal computer.

Blade torque was not directly measured in the experiments but derived from its fundamental relationship to rotational acceleration. For tests that are within the positive performance region of the VAWT, applying a brake torque was necessary to prevent the rotor from over speeding and causing structural and safety issues. A Magtrol hysteresis brake (model: HB-140-M2) was used for this purpose. As current is applied to the hysteresis brake, a magnetic field proportional to the current is established within the device producing the desired braking effect. The braking torque T_{app} is independent of the rotational speed of the rotor and as such provides a constant brake regardless of the running conditions of the VAWT. To measure the applied torque T_{app}, the brake is mounted on a spring balance and a Sangamo DC miniature displacement transducer (model: DFG/2.5) measures the linear displacement of the transducer core attached to a point on the balance with known lever arm length of 155mm from the brake centre. Although the movement of the balance is rotational, the full stroke of the displacement transducer is only 2.5mm rendering the rotational displacement practically linear. The transducer voltage was linearly proportional to the displacement and a calibration curve fit (Figure 4) was obtained by loading the system with static standard weights. Maximum error was observed to be ±0.01Nm.

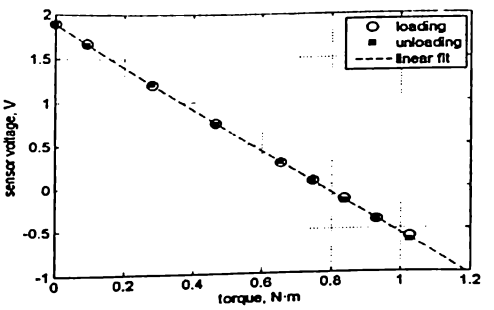

Figure 4. Calibration fit for the torque sensor.

High frequency measurement of wind speed is carried out using a constant temperature hotwire anemometer (probe model: Dantec Type 55 P16). The hotwire was positioned in the middle of the test section area and 0.4m downstream of the test section inlet. It was calibrated in situ using a highly sensitive Furness Controls FCO510 micromanometer with a stated accuracy of 0.25% between 10% (20Pa) and 100% (200Pa) of the reading scale. A Pitot–static tube was connected to micromanometer and mounted close to the hotwire. Hotwire measurements were performed across the entire tunnel cross sectional area up to 0.1m from the tunnel walls and the variations in the readings between different positions were within the measurement variation of one position. As such, flow was considered to be uniform throughout and the selected final position of the hotwire is considered acceptable and representative of the general flow velocity in the tunnel. The reference velocities for hotwire calibration were derived from the differential pressure readings using the ambient temperature from a digital thermometer and ambient pressure from a mercury barometer taken at the start of each series of tests in a day. The entire calibration procedure was conducted within 10 minutes of the ambient temperature and pressure measurements to keep the calibration data within similar conditions.

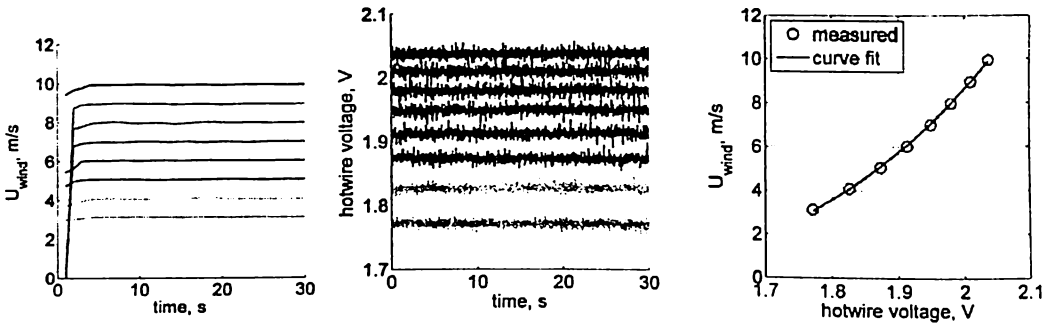

Figure 5. Hotwire calibration plots: a) wind speed calculated from differential pressure readings, b) hotwire voltage readings, c) calibration curve fit.

The tunnel fan was run at various constant speeds and at each fan speed, the flow was allowed to settle before measurements were made. A total of 8 constant wind speeds were tested covering a range of approximately 3m/s up to 10m/s. For each test wind speed, both differential pressure readings from the micromanometer and voltage readings from the hotwire were recorded for 30s. The fastest logging frequency of the micromanometer was 1Hz so this was used for all the tests. The hotwire logging frequency was tested at frequencies of 100Hz, 1000Hz, and 10,000Hz. The final logging frequency was set to 100Hz which was determined to be adequate to capture the unsteadiness in the flow velocity due to turbulence effects. During each test, the first 5 seconds of manometer data was discarded. The average of the last 25s of the manometer data and the 30s of the hotwire data were taken and used in computing for the coefficients of a simplified form of King's Law equation (1) for hotwire anemometry using a simple least–squares curve fitting method.

$$V^2 = A + B \cdot U^n \tag{1}$$

where V: hotwire voltage
U: wind speed
A, B, n: constant coefficients, n ~ 0.5

Determining the flow turbulence was an important part of the experiments as the measured turbulence was eventually used in the boundary conditions for numerical simulations not covered in this paper. With a turbulence grid in place at the start of the test section, it was necessary to find the level of turbulence of the flow at the position of the VAWT since a decay in turbulence intensity Tu is expected between these two points. The hotwire was traversed downstream in increments of 0.2m from its initial position up to near the upstream most position of the VAWT blades at 1.4m from the test section inlet. Figure 6 shows a plot of the measured Tu versus measurement position. At the initial measurement point of x = 0.4m from the test section inlet, Tu = 3.43%. It rapidly decays down to 1.80% after only a 0.4m movement downstream at x = 0.8m. By the time the wind has reached x = 1.4m, Tu has dropped to a value of 1.04%.

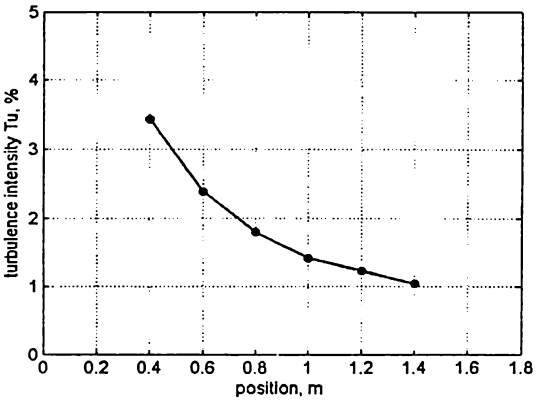

Figure 6. Turbulence intensity decay in the wind tunnel (x = 0: test section inlet).

3. RESULTS

3.1 Steady Wind Performance

Measurement of the steady blade power used an indirect method following a procedure developed by Edwards [6]. The VAWT blade performance was measured by spinning the rotor down from a high rotational speed and the deceleration monitored using the optical encoder. The instantaneous acceleration is the ratio of the change in angular speed ω over elapsed time between the two ω readings, given by

$$\xi = \frac{\omega_2 - \omega_1}{t_2 - t_1} \tag{2}$$

where ξ: angular acceleration
ω: angular speed
t: time

For each wind speed condition, two spin down tests were needed to determine the blade performance of the VAWT. The first involves the spin down of the rotor without the blades. This is necessary to determine the system resistance which includes the drag induced by the support arms, and bearing and mechanical friction. After this test, T_{res} is established via Eq. 3 for the specific wind speed that the spin down test was performed. In all resistive spin down cases, there was no need to apply a brake to the system because there was no positive performance expected without the blades attached. Also, it was seen that the resistive load of the system was independent of the wind speed, i.e. the T_{res} curves for all resistive spin down tests coincide with each other.

$$T_{res} = I_{rig}\xi \tag{3}$$

where I_{rig}: rotational mass moment of inertia.

The second spin down with the blades attached measured the full rotor performance including blade tip effects and blade–support arm junction effects. Blade torque T_B was deduced from the difference between the rotor torque $I_{rig}\xi$ and the system resistance T_{res}. It is necessary to separate the blade performance from the contribution of other design components not only for design considerations but also for direct comparison to 2D CFD models where only blades are analysed. For tests at wind speeds greater than 7m/s, the application of the hysteresis brake was required because of positive rotor performance which caused the VAWT to cut–in and not come to a full stop. Blade power was deduced by subtracting both system resistance and brake torque applied T_{app} from the rotor torque. The equation for this relationship is shown in Eq. 4.

$$T_B + T_{res} + T_{app} = I_{rig}\xi \tag{4}$$

where T_B: blade torque
T_{res}: resistive torque
T_{app}: applied brake torque
I_{rig}: rotational moment of inertia of the VAWT

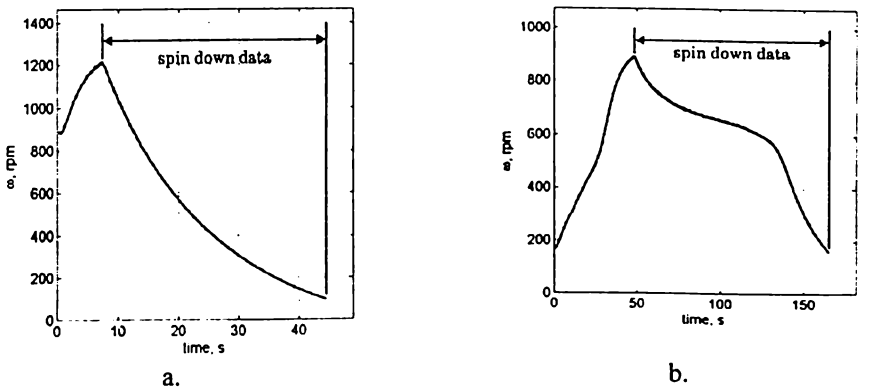

Figure 7. Sample spin down data plots: a) without blades, b) with blades.

Plots of ω versus time are shown in Figure 7 for the two spin down tests. In both tests, the rotor is spun to a high rpm corresponding to a maximum λ of almost 5 for each wind speed being tested so that full coverage of the performance curve can be obtained. Figure 7b clearly shows the influence of the blades on the rotation of the rotor. The time to spin the rotor up is much longer with the blades on than without. There is also a distinct plateau in rpm which indicates positive blade performance, counteracting the resistive loads such as mechanical friction, aerodynamic drag, and brake torque (when applicable).

An important consideration in the test assumptions is that the addition of the blades does not have an effect on the resistive loads in the system. There are several likely reasons for which this might not the case. For one, the increased weight of the rig may alter the bearing friction. To verify this, the pre–tension spring that holds the rig firmly in place was further compressed to simulate an added weight into system. Spin down tests with the additional load were conducted and the resulting T_{res} compared to the baseline case. There was no significant difference observed in the overall system resistance with the added load. Another consideration that may affect the

resistive loads in the system was the blade–support arm junction which may increase or decrease the system drag. Additionally, with the support arm ends not exposed to tip effects, a reduction in drag may be probable. Assessing the individual effects is difficult and the degree of their influence on the overall value of T_{res} is likely very small. It is assumed that the tests are satisfactory in establishing the overall resistive loads in the system.

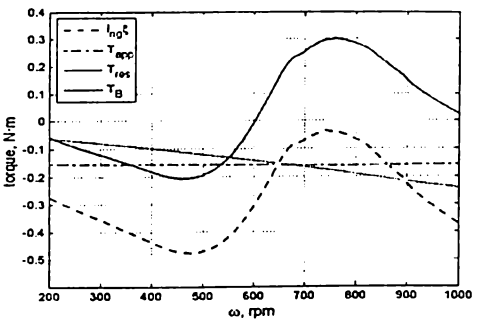

Figure 8. An illustration showing the results for the torque terms vs. ω as determined from two spin down tests at 8m/s.

Figure 8 shows a sample result for a set of spin down tests at 8m/s. The variations of the torque terms in Eq. 4 are presented versus ω covering an equivalent λ range of about 1 – 5. The total rotor torque $I_{rig}\xi$ is seen to be completely in the negative region. This is expected and necessary for the spin down to be carried out. The $T_{app} \approx -0.16$N·m is the constant braking torque applied during the complete rotor spin down test. The T_{res} is seen to increase in magnitude as ω increases. Blade torque T_B varies from the negative region at low λ to positive values above ω = 602rpm corresponding to a λ = 2.9. Maximum T_B is 0.30N·m at ω = 759rpm (λ = 3.9) while minimum T_B is –0.21N·m at ω = 462rpm (λ = 2.2).

Spin down tests were performed at different wind speeds to map the performance of the VAWT. At the start of each test, the wind speed is set whilst the rotor is stationary. During the start of the spin down test, the wind speed is observed to fall from the set speed due to blockage effects before eventually rising as the test ends (Figure 9). For the spin down test at the highest wind speed, U = 8.1m/s at the start of the spin down and rose to U = 8.75m/s at the end of the spin down. This results in a data set that does not represent a steady wind case. To correct for this deviation, multiple spin down tests were conducted from a minimum of 5m/s to a maximum of almost 9m/s (Figure 10a) and performance of steady wind speeds were interpolated (Figure 10b). The interval of wind speeds between tests was not constant but not seen as an issue. Regularity in the spacing was more desired and that the target steady wind speeds fall within the range of the measured wind speeds. For the current work, the minimum target steady wind speed was set to 5m/s, while the maximum was 8m/s. This range clearly falls within the range of all spin down tests conducted.

Performance curves for the different spin down tests are presented in Figure 10a. It is seen that the VAWT performance varies considerably with wind speed. At the lowest test wind speed, the entire CP curve is in the negative region. As the test wind speed is increased, the peak CP slowly rises above zero and continues to rise within the same λ region until it reaches a maximum of CP = 0.31 at the optimum tip speed ratio $\lambda^* = 3.9$ for the highest test wind speed. To a very small

degree, there is an observed convergence of CP curves towards higher test wind speeds especially within the low λ range. A convergence in steady CP curves as Reynolds number increases is observed suggesting an approach to independence from Reynolds number effects at higher wind speeds.

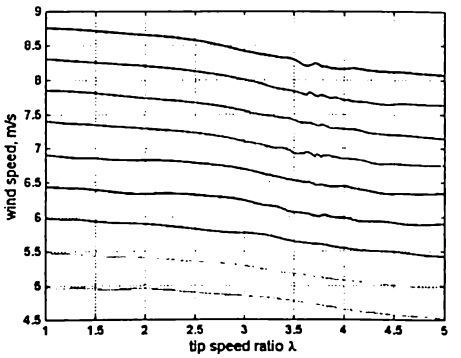

Figure 9. Drop in wind speed for each of the spin down tests.

There is a well–defined negative band appearing in the low λ range which is also seen by Edwards [6], Baker [7], Kirke [8] and McIntosh [9]. According to Baker, this negative band, which he termed as the dead band, negatively affects the self–starting capabilities of the VAWT and can be minimized by tilting the blade forward relative to the VAWT axis as well as mounting the blade at a positive yaw (re: fixing) angle. Tilting the blade effectively reduces the effective angle of attack seen by the blades which minimises the occurrence of deep stall at low λ. Edwards has shown that the yawing of the blade such that the leading edge is closer to the VAWT rotation axis causes earlier stall at low λ but the depth of stall is reduced. The effect on the overall performance is a slight increase in CP in the dead band but a significant decrease in CP within the positive performance band. Kirke showed that as the Reynolds number is reduced, there is a deepening of the dead band and the lowering of the overall performance of the VAWT. In his parametric studies, McIntosh demonstrated that a dead band will appear when the stall angle of the aerofoil is reduced. This concurs with Baker's conclusion that lower stall angles induce deeper dead bands typically seen in thinner aerofoil sections or at low Reynolds number conditions.

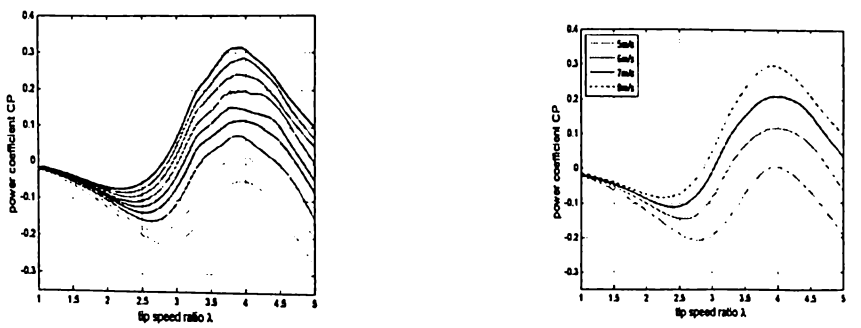

a. b.

Figure 10. CP curves for the spin down tests: a) actual CP curves for all tests, b) interpolated CP curves for steady wind speeds.

Figure 10b shows the interpolated curves for constant wind speeds. A convergence is also seen in the curves as wind speed increases. When compared to the data presented by Edwards [6], the maximum value of the interpolated CP for the 7m/s case is higher at 0.21 than the non–interpolated case at 0.14. This is so because at the λ^*, the actual wind speed in the spin down test has dropped to just above 6.5m/s. So the CP value of 0.14 corresponds to this reduced wind speed and not the performance at 7m/s. Despite this difference, the general trends in the CP curve are still similar between the two studies. At low λ, the performance is driven by the drag on the blades producing a deep dead band with the lowest CP of –0.11 at $\lambda = 2.4$ (Figure 11). Subsequently, a rapid increase in CP is observed until the CP crosses the zero line at $\lambda = 3$ and continues to rise until it reaches the maximum value of 0.21 at $\lambda^* = 4.0$. Beyond λ^*, the CP rapidly drops to 0.03 at $\lambda = 5$.

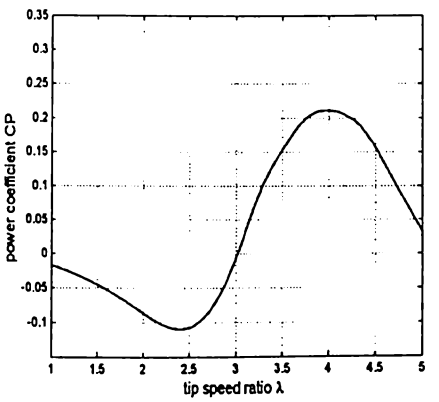

Figure 11. Steady wind performance curve at 7m/s.

4. CONCLUSIONS

The spin down technique has shown to be an invaluable tool in the fundamental understanding of VAWT performance in steady wind conditions. The performance of the VAWT in 7m/s steady wind over a wide range of λ is revealed to have a negative trough from $\lambda = 1$ up to $\lambda = 3$ with the lowest CP of –0.11 at $\lambda = 2.4$. Beyond $\lambda = 3$ the CP rises until the maximum value of 0.21 at $\lambda^* = 4.0$ after which it falls close to zero at $\lambda = 5$. This CP profile is typical of the scale of the VAWT tested where a negative trough is present mostly due to high zero–lift drag that hampers the ability of the rotor to generate positive torque at low λ and self–start. The negative trough is observed to slowly diminish as wind speeds, and consequently, Reynolds number increases.

Nomenclature

A	rotor frontal swept area, 2RL	U_∞	free stream wind speed
c	blade chord		
CP	power coefficient	λ	tip speed ratio, $R\omega/V_\infty$
I_{rig}	rotor rotational mass moment of inertia	λ^*	tip speed ratio at maximum CP
L	blade length	ξ	rotor angular acceleration
N	number of blades	ρ	air density
P_B	blade power	σ	rotor solidity, Nc/R
P_w	wind power	ω	rotor angular speed
R	rotor radius		
T_{app}	applied brake torque	HAWT	horizontal axis wind turbine
T_B	blade torque	VAWT	vertical axis wind turbine
T_{res}	resistive torque		

RFERENCES

[1]"Climate Change 2007: The Physical Science Basis," Technical Report No. AR4, Intergovernmental Panel on Climate Change, Cambridge, United Kingdom and New York, NY, USA.

[2] Department of Energy Change and Climate. Renewable Energy in 2011, June 2012, Accessed online 31 August 2012, http://www.decc.gov.uk.

[3] Department of Energy Change and Climate. UK Energy in Brief 2012, July 2012, Accessed online 31 August 2012, http://www.decc.gov.uk.

[4] Iida, A., Mizuno, A., and Fukudome, K., 2004, "Numerical Simulation of Aerodynamic Noise Radiated Form Vertical Axis Wind Turbines," The 18th International Congress on Acoustics, Kyoto, Japan.

[5] Mertens, S., Van Kuik, G., and Van Bussel, G., 2003, "Performance of an H-Darrieus in the Skewed Flow on a Roof," Journal of Solar Energy Engineering, 125(4), pp. 433-440.

[6] Edwards, J., 2012, "The Influence of Aerodynamic Stall on the Performance of Vawt Blades," Ph.D. thesis, University of Sheffield, Sheffield.

[7] Baker, J. R., 1983, "Features to Aid or Enable Self Starting of Fixed Pitch Low Solidity Vertical Axis Wind Turbines," Journal of Wind Engineering and Industrial Aerodynamics, 15(1–3), pp. 369-380.

[8] Kirke, B. K., 1998, "Evaluation of Self-Starting Vertical Axis Wind Turbines for Stand-Alone Applications," Ph.D. thesis, Griffith University, Gold Coast, Australia.

[9] Mcintosh, S. C., 2009, "Wind Energy for the Built Environment," Ph.D. thesis, Cambridge University, Cambridge.